A flexible polymer–nanoparticle hybrid material containing triazole-based Fe(ii) with spin crossover properties for magneto-optical applications

Hugo Voisin, Carole Aimé, Anne Vallée, Thibaud Coradin, Cécile Roux

A flexible polymer–nanoparticle hybrid material containing triazole-based Fe(II) with spin crossover properties for magneto-optical applications†

Hugo Voisin,‡ Carole Aimé, Anne Vallée,§ Thibaud Coradin * and Cécile Roux*

In the perspective of elaborating functional devices based on inorganic molecular materials, it is important not only to continue research on their synthesis and to understand their properties but also to develop new strategies for their processing and shaping. In this context, we show here that centimeter-scale materials exhibiting solid state-like spin-crossover (SCO) properties and easy handling under ambient conditions can be obtained that preserve their thermochromic properties over months. Combining a triazole-based Fe(II) SCO compound with functionalized silica nanoparticles gives rise to nanocomposite soft gels. These gels were used as templates for the formation of a flexible macroporous hybrid silica network *via* a vapor phase sol–gel process. Further coating with PDMS provided both long-term protection of the material against drying and operationality in aqueous media. Our approach offers new hopes for the development of optical and magnetic devices based on SCO coordination polymers.

1. Introduction

The spin-crossover (SCO) phenomenon found in coordination compounds originates from the existence of metal–ligand interactions of intermediate strength, allowing for a stimuli-induced reversible switch from the high spin state (HS) to the low spin (LS), associated with profound modifications of their magnetic and optical properties making them very attractive for sensors, data storage or magneto-optical displays.[1–3] Among SCO materials, the one-dimensional triazole-based Fe(II) family with the general formula $[Fe(R\text{-}Trz)_3](A)_{2/x}$ (with R-Trz = 1,2,4-triazole ligand functionalized in the 4-position by an R group and A^{x-} = counter-anion) is quite unique as it shows an abrupt transition, and is sometimes associated with wide thermal hysteresis around room temperature.[4–6] This is indicative of a high degree of cooperativity resulting from the bridging of triazole ligands. In the solid state, SCO characteristics (transition temperature and hysteresis width) depend on structural (intermolecular interactions and polymorphism) and chemical factors (ligands, counter-anions, and solvents) allowing one to obtain a broad diversity of compounds. In particular, the water molecule content can induce drastic changes in the SCO properties.[7–12] Key difficulties in converting these materials into functional devices are the low solubility of SCO compounds and the preservation of the SCO cooperativity, in particular in water, which is necessary for a broad range of applications. This explains why the diversity of SCO molecular structures is lost in SCO devices.

Over the past two decades, SCO materials were prepared as thin films,[13–17] liquid crystals,[18,19] and nanostructured objects.[20–26] Supramolecular gels have also been successfully obtained based on the alkyl functionalization of triazole ligands and/or counter-anions,[27–33] with few examples using hydrophilic ligands[34,35] or a polyol synthetic route.[36] The latter approach may be of particular interest as it should extend the possibility of obtaining gels from a broad diversity of SCO systems reported in the literature. In particular, we have recently used this polyol route combined with a hybrid approach. We have reported the synthesis of nanostructured hybrid gels (Si–SCO) that combine silica nanoparticles (NPs) with amorphous and microcrystalline SCO polymers $[Fe(A\text{-}Trz)_3]SO_4$ (with A-Trz = 4-amino-1,2,4-triazole). We have shown that the presence of NPs and the subtle balance between the three interacting components is a unique way to control the SCO properties of the gel.[36] In this case, transition

Sorbonne Université, CNRS, Collège de France, Laboratoire de Chimie de la Matière Condensée de Paris, F-75005 Paris, France. E-mail: cecile.roux@upmc.fr

†Electronic supplementary information (ESI) available: Detailed experimentals for Step 1, DSC and magnetic behaviors of the Si-SCO composite and the SCO system, DSC characterization of Si@Si-SCO aged for 28 days, XRPD of the Si-SCO composite system and of its compounds, XRPD of the Si-SCO and Si@Si-SCO systems and substraction of the amorphous background. See DOI: 10.1039/c8qi00494c

‡Present address: Department of Materials and Environmental Chemistry, Stockholm University, SE-10691 Stockholm, Sweden.

§Present address: Institut Lavoisier de Versailles, UMR 8180, Université Paris-Saclay, Université de Versailles Saint-Quentin, 45 avenue des Etats-Unis, 78035 Versailles Cedex, France.

temperatures (heating $T^{\nearrow}$ and cooling $T^{\searrow}$) have been shown to increase with increasing SiO_2 content (Fig. S1 and S2†).

However, the integration of switchable molecular systems as active elements into 3D centimeter-scale devices remains a challenge.[37] This is due to the fact that despite the purely molecular origin of the SCO phenomenon, the macroscopic behavior of these systems is strongly influenced by short- and long-range interactions between the transition-metal ions, giving rise to remarkable cooperative phenomena, which are in turn responsible for the robustness of the spin transition.[38–40] The engineering of composite materials is a promising way to address this ultimate goal. In this frame, SCO compounds have been encapsulated within polymer matrices of synthetic[41–49] and biological[38,50–53] origin, providing nanoscale confinement suitable for maintaining cooperativity between SCO complexes. Sol–gel techniques were also used for encapsulation. These soft chemistry routes offer a unique versatility and processability for the engineering of hybrid materials.[54] Silica porous matrices have been preformed before the addition of SCO compounds that impose an important structural constraint and limit the loading and homogeneity of the composite material.[55] Nano-composite matrices have also been formed *in situ* by mixing alkoxysilanes with an SCO nanoparticle suspension leading to brittle materials with important changes of the spin transition properties.[56] We propose here an alternative strategy where the Si–SCO gel acts as a template for the growth of a silica coating by a post-diffusion route. This strategy is particularly well-suited for fragile objects.[57] In this work, we demonstrate that bulk materials exhibiting solid state-like SCO properties and amenable to easy handling and use in aqueous media can be prepared using a combination of liquid and vapor-phase sol–gel chemistry and a final PolyDiMethylSiloxane (PDMS) coating step.

2. Experimental

2.1. Synthetic procedures

Step 1. Synthesis of the Si–SCO composite

Silica NPs functionalized with sulfonate groups. Silica NPs were synthesized following the Stöber process. Sulfonate functionalization of the surface proceeded through a previously described two-step procedure.[36] Zeta potential and size distribution are systematically measured using a Malvern Zetasizer Nano ZS90 instrument giving a negative zeta potential of *ca.* −53 mV in 0.5 M acetic acid (pH 2.5) and a hydrodynamic diameter of *ca.* 200 nm.

Preparation of the Si–SCO composite. As previously described,[36] 140 mg of silica NPs (200 nm in diameter) were suspended in 0.75 mL of an ethylene glycol : water mixture (v/v 9 : 1) under sonication for 45 minutes. 27.8 mg of iron sulfate heptahydrate ($FeSO_4{\cdot}7H_2O$, 0.1 mmol) (Sigma-Aldrich, 99%) were added to the suspension and heated at 50 °C for 30 minutes with 20 mg of ascorbic acid. In parallel, 50.4 mg (0.6 mmol) of 4-amino-1,2,4 triazole (ATrz, $C_2H_4N_4$, Alfa-Aesar, 99%) was separately dissolved in 0.25 mL of the same ethylene glycol : water mixture at RT. After completion of the dissolution of the iron salt, the ATrz solution was placed in an ice bath and the NP–$FeSO_4$ solution was added dropwise under stirring. The final content of Fe^{2+} ions was 0.1 mol L^{-1} (0.42% w/w). This corresponds to a proportion of silica (SiO_2) to SCO polymer of 23.

Step 2. Si@Si–SCO: exposition to alkoxysilane vapors. Immediately after mixing the iron salt and the aminotriazole solutions, the resulting viscous suspension was casted in a PolyTetraFluoroEthylene (PTFE) mold of dimension typically 50 × 25 × 2 mm before being left to age in a closed chamber at RT for 9 days (Fig. 1b, Step 1). The mold with the Si–SCO composite was then introduced in a desiccator of which the bottom was filled with an organosilane. The closed desiccator was then placed in an oven at 25 °C (Fig. 1b, Step 2). The molds filled with Si–SCO composites were left open to silane vapors in the desiccator for a variable duration.

Step 3. Si@Si–SCO: aging. Once the exposure time was reached, the molds were taken out of the desiccator to be stored in a closed chamber at RT (Fig. 1b, Step 3). Their macroscopic aspect was monitored during their aging.

Step 4. PDMS@Si@Si–SCO: coating. PDMS coating of the Si@Si–SCO composites (Fig. 1b, Step 4) was carried out using commercial Bluesil RTV 141 (Bluestar Silicones). A PTFE mold was realized with slightly bigger dimensions than the piece of the material to be coated. A thin layer (1 mm) of the mixture of the constituents A and B of the silicone was laid down on the bottom of the mold before being degassed under vacuum. The layer was reticulated at 70 °C for 30 minutes. The piece of Si@Si–SCO material was then put on the hardened layer before being covered by a mixture of the constituents A and B of the silicone. The system was then degassed, before being reticulated at 70 °C for 30 minutes. The PDMS coated material could then be taken out for further characterization.

2.2. Crystallisation of the polymer in ethanol

The silica-free SCO polymer was prepared in an ethylene glycol : water mixture (v/v 9 : 1) as previously described.[36] To this suspension, 10 mL ethanol was added to induce the formation of a precipitate. The mixture was centrifuged, washed 3 times with 10 mL ethanol and the precipitate was recovered before drying under ambient air.

2.3. Differential scanning calorimetry

DSC measurements were performed on a TA Instruments model Q20 system. Aluminum capsules were loaded with 20–50 mg of Si–SCO and Si@Si–SCO samples and sealed. In the case of PDMS@Si@Si–SCO, the coating was directly performed within the capsule before sealing. The set-up and enthalpies were calibrated with respect to temperature using an indium reference (430 K, 3.3 J mol^{-1}). Cooling and heating sweeps were performed at a scanning rate of 5 K min^{-1} under a N_2(g) atmosphere. The transition temperatures were derived by considering the maximum of the thermal anomalies.

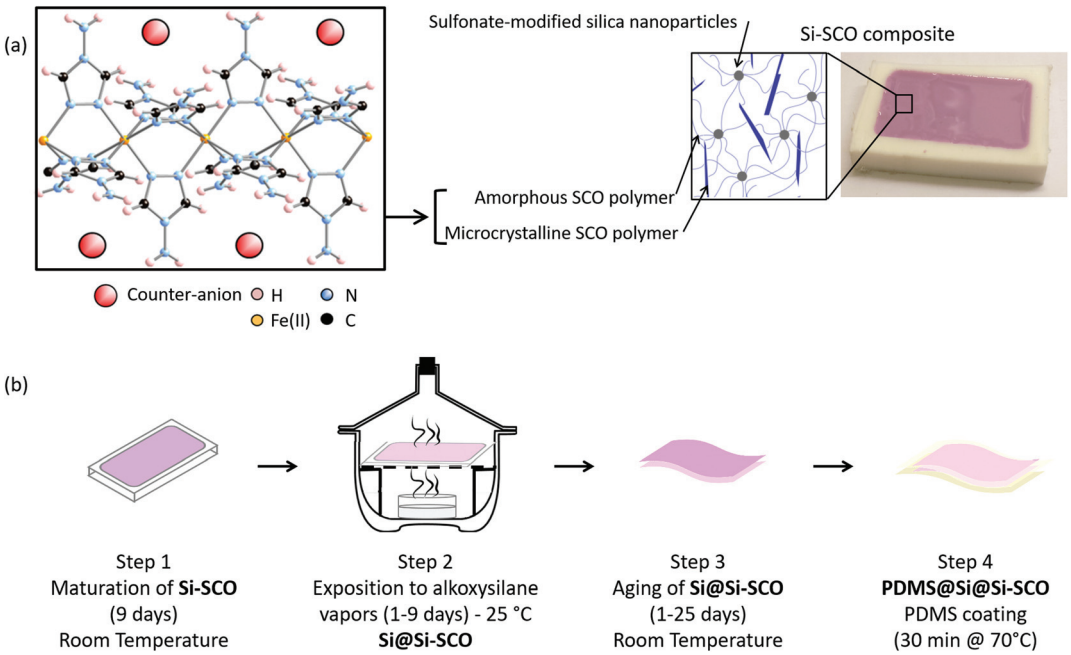

Fig. 1 (a) Structure of the SCO polymer $[Fe(A\text{-}Trz)_3]SO_4$, and schematic representation and photograph of Si–SCO. (b) Scheme of the processing steps from Si–SCO (Step 1) to PDMS@Si@Si–SCO (Step 4).

2.4. X-ray powder diffraction

XRPD measurements were carried out using the Cu Kα1 radiation on a Philips PW 1830 diffractometer. The samples were deposited on an Si monocrystal in order to have a flat background.

2.5. Dynamic mechanical analysis

The analysis was conducted on an MCR 302 Anton-Paar rheometer equipped with a solid rectangular fixture, SRF12. After diffusion of the silane vapour inside the composite gel and aging of the material, it was taken out of the PTFE cast and cut in pieces of dimensions typically 40 × 10 × 2 mm. The strips were then placed in between the instrument grips before being subjected to a strain sweep from 0.1% to 100% at a constant excitation frequency of 0.1 Hz. All experiments and their corresponding measurements were conducted in triplicate.

2.6. Electron microscopy

Scanning electron microscopy (SEM) imaging was performed using a Variable Pressure Hitachi S-3400N microscope after depositing a thin layer of the sample on aluminium pads without any further metallization.

3. Results and discussion

As previously described,[36] the Si–SCO system consists of a tripartite gel in ethylene glycol/water (v/v 90/10) with sulfonate-modified silica NPs and amorphous and microcrystalline SCO polymers $[Fe(A\text{-}Trz)_3]SO_4$ (with A-Trz = 4-amino-1,2,4-triazole) (Fig. 1a). Very importantly the subtle balance between these three interacting components allows reaching similar SCO properties as those of the $[Fe(A\text{-}Trz)_3]SO_4$ coordination polymer in the solid state ($T^{\nearrow}$ = 328 K; $T^{\searrow}$ = 312 K, Fig. 4c and S1†). While the spin transition finds its origin in the crystalline phase, it also induces a spin change in the amorphous phase favoured by the presence of silica NPs (Fig. S2†).

The Si–SCO composite gels can be casted into PTFE molds before gelation. The gel then evolves significantly over 9 days at 25 °C with an increasing amount of the crystalline phase, hence of the SCO properties. The purple color is characteristic of the low spin state of the SCO polymer (Fig. 1a and b, Step 1). From this maturation state, the composite SCO gel exhibits a very good stability over months for both mechanical and SCO properties, although with relatively poor rheological properties (storage modulus G' = 8–10 kPa). This high stability makes our mature SCO gel a very robust template for the post-diffusion of alkoxysilanes. Exposing samples to a silica precursor in the vapor phase to induce the sol–gel reaction is a technique commonly used to deposit silica thin films *in situ* at the surface of fragile samples without destroying their structure.[58] The Si–SCO gel was placed into a desiccator saturated with organosilane vapors (Fig. 1b, Step 2). Variations in the nature of the precursor have shown that for all organosilanes, solvent expulsion is systematically observed due to silica condensation. Organosilanes bearing a chemically reactive organic function, such as amino- or glycidopropyltriethoxysilane, oxidized the iron(II) ions thus destroying the coordination polymer (Fig. 2a). As a result, we observe the loss of thermochromism (low spin purple/high spin white). In contrast, the use of tetraalkoxysilanes, such as tetraethoxysilane (TEOS) or tetramethoxysilane (TMOS), resulted in a silica matrix

(a)

Thermo chromism	Macroscopic aspect	Alkoxysilane
✗	Gel	(3-Chloropropyl)triethoxysilane ; (3-Aminopropyl)triethoxysilane ; (3-Glycidyloxypropyl)triethoxysilane
✓	Brittle solid	Tetramethoxysilane (TMOS) ; Tetraethoxysilane (TEOS)
✓	Flexible solid	Methytriethoxysilane (MTEOS)
✓	Sticky solid	Phenyltriethoxysilane
✓	Viscous Liquid	Dimethyldimethoxysilane ; 1,2-Bis(triethoxysilyl)ethane ; 1,4-Bis(triethoxysilyl)benzene

(b)

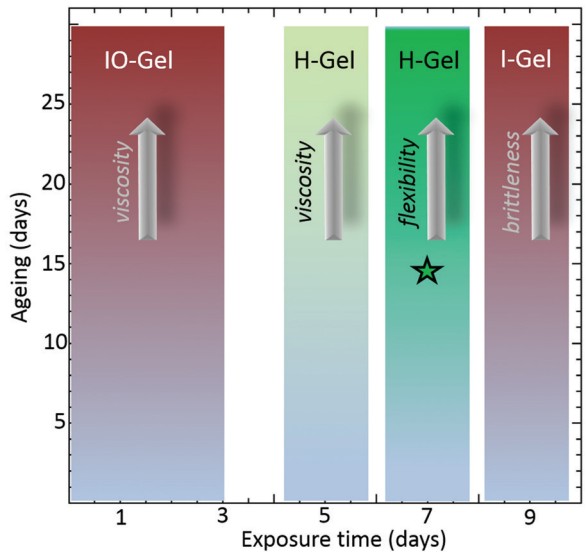

Fig. 2 (a) Table describing the characteristics (thermochromism and macroscopic aspect) of Si@Si–SCO samples obtained after exposition at 25 °C of 9 days mature Si–SCO gel. Green and red check marks correspond to an observable thermochromism (purple-white color change as a function of the temperature) or not, respectively. (b) Graphical representation of the macroscopic aspect of Si@Si–SCO samples as a function of exposure time to MTEOS and aging at 25 °C of the 9 days mature Si–SCO gel. IO-Gel = inhomogeneous oxidized gel; H-Gel = homogeneous gel; I-Gel = inhomogeneous gel. The star mark corresponds to the optimized parameters for the obtention of thermochromic flexible materials.

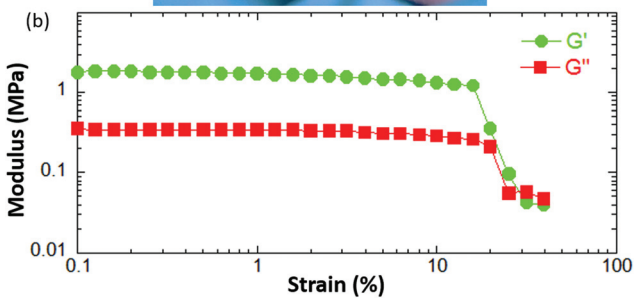

Fig. 3 (a) Photograph of Si@Si–SCO after 1 week of exposure and 14 days of aging. (b) An associated rheological profile under shear stress at a fixed excitation frequency of 0.1 Hz.

that was found to be too rigid to accommodate with the condensation-induced stress, leading to brittle materials. Alkyltrialkoxysilanes were thus used, with methyltriethoxysilane (MTEOS) leading to materials with optimal mechanical behavior. It is important to note that the presence of silica NPs is necessary to obtain a homogeneous material. In the absence of silica NPs, phase separation was observed during exposition to MTEOS vapors. Exposure time also had a strong influence on the material. In particular, short expositions (less than 3 days) led to inhomogeneous fragile gels that become oxidized with time after 25 days (Fig. 2b). Beyond 8 days of reaction, inhomogeneous gels were also obtained but without oxidation. In this case, important solvent expulsion from the material was observed together with its shrinkage, which can be attributed to an excessive condensation of the silica network.

In contrast, homogeneous gels can be obtained for intermediate exposure times (between 5 and 7 days) exhibiting a purple color and the thermochromism characteristic of the SCO phenomenon. After 5 days exposure, the increasing viscosity upon aging leads to pasty gels. This can be improved by increasing the exposure time to 7 days leading to centimeter-scale flexible and easy to handle samples (Si@Si–SCO, Fig. 3a). Material flexibility at the macroscopic scale is reached after 15 days of aging. At this point, the gel state is confirmed by dynamic mechanical analysis with a storage modulus of *ca.* 1 MPa, which is higher than the loss modulus of 0.4 MPa (maximum deformation of 15%, Fig. 3b). This is three orders of magnitude higher than our previously reported hybrid system before exposure,[36] and more than four orders of magnitude higher to what is commonly reported for pure SCO gels.[28]

The XRPD analysis of Si@Si–SCO shows two broad peaks at 2θ = 11 and 23° that are characteristic of the amorphous polymer and silica (Fig. S4†). In addition, well-defined diffraction peaks corresponding to the solid SCO polymer alone are observed for Si@Si–SCO, which were also preserved in the Si–SCO nanocomposite (Fig. 4a and Fig. S5, S6†). This reveals that the crystalline structure of the coordination polymer was not affected by the formation of the silica matrix. Characterization of the SCO properties of the Si@Si–SCO material was performed using the calorimetric method (DSC). Upon heating, a broad endothermic peak was observed at $T^{\nearrow}$ = 333 K associated with the LS/HS transition. A broad exothermic peak at $T^{\searrow}$ = 316 K upon cooling is observed for the HS/LS transition (Fig. 4b). This is characteristic of a first order transition with a hysteresis width of 17 K. These values are similar to those of the Si–SCO system (Fig. 4c). The small increase in temperature observed for Si@Si–SCO can be attributed to the limited reorganization of the amorphous phase in the tri-partite system.

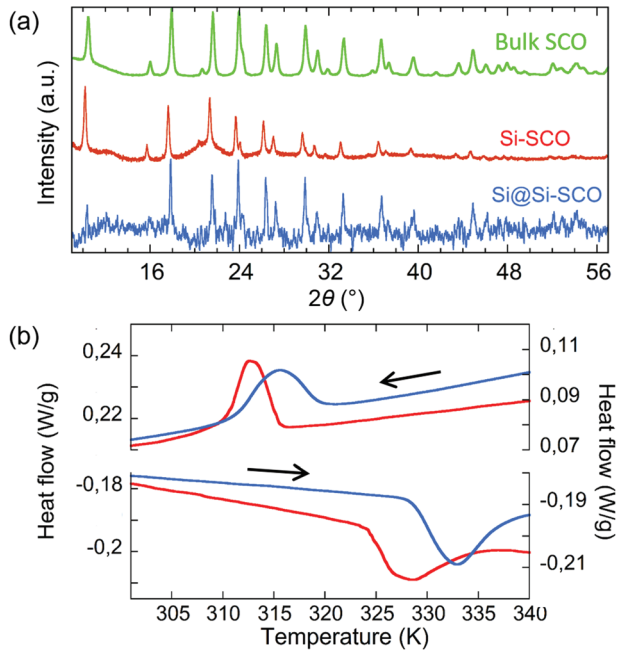

(c)

Samples	$T^{\uparrow}_{max}$ (K)	$T^{\downarrow}_{max}$ (K)	ΔH (kJ.mol^{-1})
SCO suspension[36]	325	310	*Not determined*
Mature Si-SCO gel[36]	328	312	12.5
Si@Si-SCO	333	316	9.1
PDMS@Si@Si-SCO	328	312	8.4
PDMS@Si@Si-SCO Aged 80 days	331	316	7.5

Fig. 4 (a) XRPD diffractograms of Si–SCO and Si@Si–SCO by deducing the amorphous phase (Fig. S5 and S6†). For comparison, the diffractogram of solid SCO without silica is plotted in green. (b) DSC at 5 K min^{-1} of Si–SCO (red lines) and of Si@Si–SCO (blue lines) aged for 14 days. DSC thermographs plotted as "exo up". (c) SCO characteristics from DSC results for the different samples.

Given the solvent evaporation, the iron concentration is estimated to be 0.5% w/w. The corresponding ΔH for the LS/HS transition can be evaluated to be 9.1 kJ mol^{-1}. This value is slightly lower than that of the integrated ΔH for the mature Si-SCO gel before alkoxysilane exposure.

SEM observations showed the presence of needle-shaped crystalline objects (Fig. 5a, white circles) and spherical nanoparticles (Fig. 5a, yellow arrows), reminiscent of the Si–SCO system (Fig. 5c), located within the cavities of a macroporous silica-based matrix. This model is schematically depicted in Fig. 5b. This supports the hypothesis that silane condensation occurs in the ethylene glycol solvent phase, around Si–SCO composite domains. The similarity of these results with those of the Si–SCO system shows that (1) the sample microstructure and thus the SCO amorphous and crystalline organizations are not significantly affected by the sol–gel reaction, and (2) the macroscopic flexibility of the silica matrix preserves the molecular elastic interactions between the iron sites.

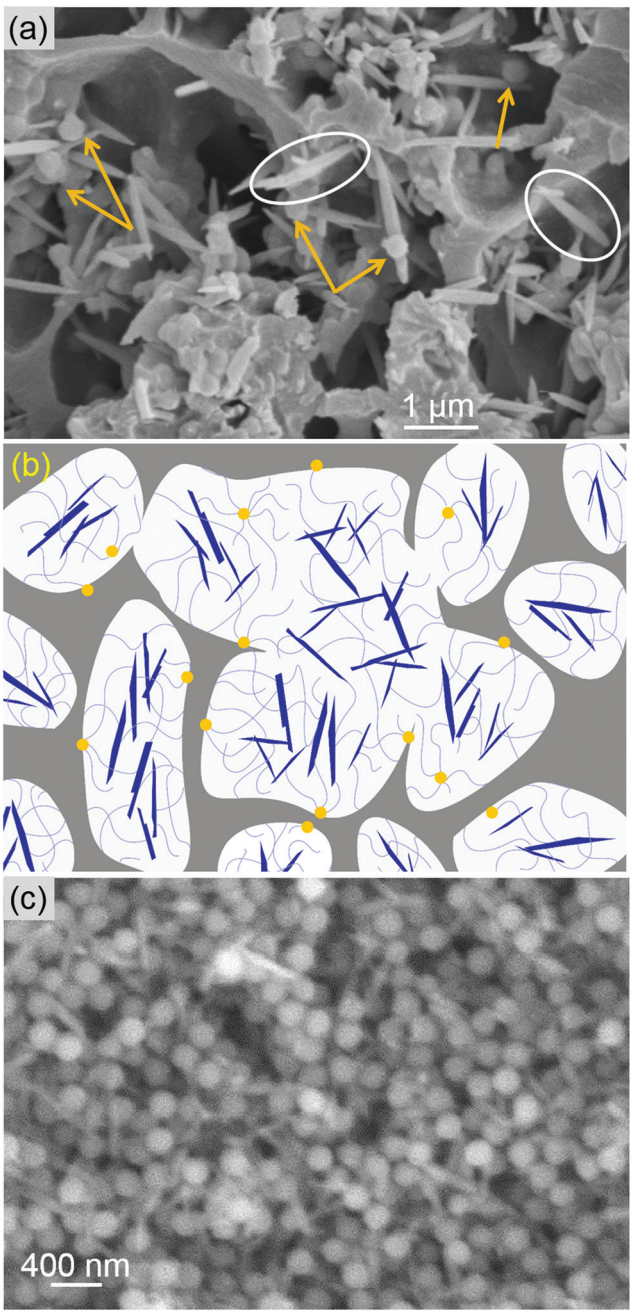

Fig. 5 SEM images of (a) Si@Si–SCO (yellow arrows highlight the silica NPs, white circles the microneedles) aged for 14 days. (b) Scheme of the structure of Si@Si–SCO (the grey background represents the organosilica matrix, yellow disks the silica NPs, dark blue needles the crystalline SCO objects and light purple lines the amorphous SCO network). (c) SEM images of Si–SCO.

However, we noticed that the material evolved during the days following its preparation, and its pink color faded after 28 days (Fig. 6a). In addition, the material became brittle after 50 days due to solvent expulsion (Fig. 6b). The color change could be attributed to the decrease in the amount of LS species. However, DSC measurements performed on Si–SCO and Si@Si–SCO after 28 days show similar profiles (Fig. S3†). This

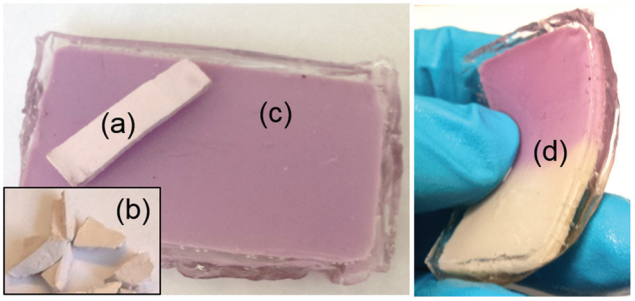

Fig. 6 Photographs of Si@Si–SCO after (a) 28 and (b) 50 days aging and (c) PDMS@Si@Si–SCO 80 days after their preparation. (d) Photograph illustrating the preserved thermochromic behavior of the flexible coated material PDMS@Si@Si–SCO.

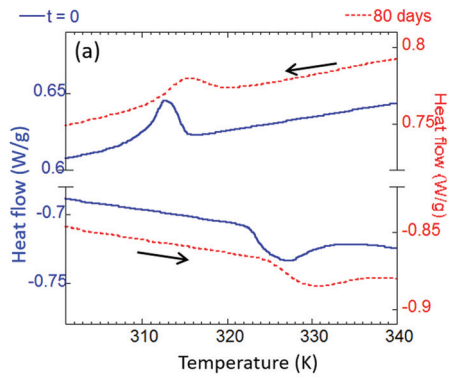

(c)

N° cycle	$T^{\uparrow}_{max}$ (K)	$T^{\downarrow}_{max}$ (K)	$\Delta H^{\uparrow}$ (kJ.mol^{-1})
1	327.70	311.04	9.9
2	327.95	311.33	10.8
3	327.95	311.29	10.8
4	327.84	312.35	9.6
5	327.89	312.61	10.3
6	327.80	312.55	10.0
7	327.54	311.79	8.8
8	327.73	311.70	9.7
9	327.50	311.87	10.0
10	327.40	311.92	9.8
11	327.46	311.89	10.1
12	327.61	312.47	9.7
13	327.47	311.98	9.9
14	327.60	312.19	10.1
15	327.35	312.05	10.3

Fig. 7 DSC characterization of PDMS@Si@Si–SCO (from 263 to 353 K at 5 K min^{-1}): (a) with aging and (b) during thermal cycles. DSC thermographs are plotted as "exo up". (c) SCO characteristics over 15 temperature cycles.

shows that the crystalline phase is not affected and rather suggests a reorganization of the amorphous phase upon solvent expulsion. In addition, the presence of the silica matrix may contribute to the whitening of the final material and the loss of color contrast between the two spin states. To limit solvent evaporation, the Si@Si–SCO material was coated after 14 days of aging with a thin layer of PDMS reticulated at 70 °C for 30 min. The coated piece exhibited far better resilience against aging 80 days after preparation when compared to the uncoated sample (Fig. 6c). This coating also allowed plunging the sample into hot water without decomposition, highlighting the pronounced thermochromism of the material (Fig. 6d). The thermochromism phenomenon is associated with an LS/HS transition that occurs at $T^{\nearrow}$ = 331 K associated with a ΔH of 7.5 kJ mol^{-1} and at $T^{\searrow}$ = 316 K as confirmed by DSC (Fig. 7a). Moreover the material displayed excellent preservation of its SCO behavior over 15 temperature cycles. From the second to the fifteenth cycle, $T^{\nearrow}$ decreases from 327.95 to 327.35 K with a variation of 0.18%. In parallel, $T^{\searrow}$ increases from 311.33 to 312.05 K with a variation of 0.23% (Fig. 7b and c). The ΔH associated with heating is considered constant at a value of 10 kJ mol^{-1}. This value is much closer to that of the fresh Si@Si–SCO gel than to that of the aged one (9.1 *vs.* 7.5 kJ mol^{-1}, Fig. 4c) showing the good preservation of the Si@Si–SCO properties.

4. Conclusions

In conclusion, we show that hybrid materials consisting of organosilica-reinforced nanocomposite gels can exhibit SCO properties similar to their parent coordination polymer in the solid state. Moreover, when properly protected by a hydrophobic coating, these materials display a unique stability over time and cycling, under ambient conditions. Our approach is therefore very promising to achieve fully functional devices based on SCO properties. Further improvements in terms of the SCO compound content of the material, as well as transition temperature and hysteresis width are now required, taking advantage of both the versatility of our process and the wide variety of SCO systems described in the literature.

Conflicts of interest

There are no conflicts to declare.

Acknowledgements

The authors thank Isabelle Genois for her constant support for SEM imaging. H. V. thanks the ED 397 at the UPMC for a PhD grant.

Notes and references

1 *Spin Crossover in Transition Metal Compounds I–III*, ed. P. Gütlich and H. A. Goodwin, Springer, Berlin, 2004, vol. 233–235.
2 P. Guionneau, *Dalton Trans.*, 2014, **43**, 382.
3 K. S. Kumar and M. Ruben, *Coord. Chem. Rev.*, 2017, **346**, 176.
4 O. Roubeau, *Chem. – Eur. J.*, 2012, **18**, 15230.
5 J. Kröber, E. Codjovi, O. Kahn, G. Grolière and C. Jay, *J. Am. Chem. Soc.*, 1993, **115**, 9810.
6 M. M. Dîrtu, A. D. Naik, A. Rotaru, L. Spinu, D. Poelman and Y. Garcia, *Inorg. Chem.*, 2016, **55**, 4278.
7 J. Kröber, J.-P. Audière, R. Claude, E. Codjovi, O. Kahn, J. G. Haasnoot, F. Grolière, C. Jay, A. Bousseksou, J. Linarès and F. Varret, *Chem. Mater.*, 1994, **6**, 1404.
8 H. Kamebuchi, A. Nakamoto, T. Yokoyama and N. Kojima, *Bull. Chem. Soc. Jpn.*, 2015, **88**, 419.
9 M. B. Bushuev, D. P. Pishchur, I. V. Koralkov and K. A. Vinogradova, *Phys. Chem. Chem. Phys.*, 2017, **19**, 4056.
10 T. Zhao, L. Cuignet, M. M. Dîrtu, M. Wolff, V. Spasojevic, I. Boldog, A. Rotaru, Y. Garcia and C. Janiak, *J. Mater. Chem. C*, 2015, **3**, 7802.
11 F. J. Muñoz-Lara, A. B. Gaspar, M. C. Muñoz, A. B. Lysenko, K. V. Domasevitch and J. A. Real, *Inorg. Chem.*, 2012, **51**, 13078.
12 E. Llobet, R. Barberà-Brunet, C. Etrillard, J. F. Létard and H. Debéda, *Procedia Eng.*, 2014, **87**, 132.
13 K. Kumar, M. Studniarek, B. Heinrich, J. Arabski, G. Schmerber, M. Bowen, S. Boukari, E. Beaurepaire, J. Dreiser and M. Ruben, *Adv. Mater.*, 2018, **11**, 1705416.
14 G. Bovo, I. Bränlich, W. R. Caseri, N. Stingelin, T. D. Anthopoulos, K. G. Sanderman, D. D. C. Bradley and P. Stavrinou, *J. Mater. Chem. C*, 2016, **4**, 6240.
15 S. Cobo, G. Molnár, J. A. Real and A. Bousseksou, *Angew. Chem., Int. Ed.*, 2006, **45**, 5786.
16 V. Shalabaeva, M. Mikolasek, M. D. Manrique-Juarez, A.-C. Bas, S. Rat, L. Salmon, W. Nicolazzi, G. Molnár and A. Bousseksou, *J. Phys. Chem. C*, 2017, **121**, 25617.
17 O. Lasco, M. L. Boillot, A. Bellec, R. Guillot, E. Rivière, S. Mazerat, S. Nowak, D. Morineau, A. Brosseau, F. Miserque, V. Repain and T. Mallah, *J. Mater. Chem. C*, 2017, **5**, 11067.
18 M. Seredyuk, A. B. Gaspar, V. Ksenofontov, S. Reiman, Y. Galyametdinov, W. Haase, E. Rentschler and P. Gütlich, *Chem. Mater.*, 2006, **18**, 2513.
19 A. B. Gaspar and M. Seredyuk, *Coord. Chem. Rev.*, 2014, **268**, 41.
20 M. Giménez-Marqués, M. L. Garcia-Sanz de Larrea and E. Coronado, *J. Mater. Chem. C*, 2015, **3**, 7946.
21 A. Rotaru, F. Varret, A. Gindulescu, J. Linares, A. Stancu, J. F. Létard, T. Forestier and C. Etrillard, *Eur. Phys. J. B*, 2011, **84**, 439.
22 K. Otsubo, T. Haraguchi and H. Kitagawa, *Coord. Chem. Rev.*, 2017, **346**, 123.
23 B. Weber, *Chem. – Eur. J.*, 2017, **23**, 18093.
24 I. Boldog, A. B. Gaspar, V. Martínez, P. Pardo-Ibañez, V. Ksenofontov, A. Bhattacharjee, P. Gütlich and J. A. Real, *Angew. Chem., Int. Ed.*, 2008, **47**, 6433.
25 G. Molnár, S. Rat, L. Salmon, W. Nicolazzi and A. Bousseksou, *Adv. Mater.*, 2018, **5**, 17003862.
26 Y.-H. Luo, Q.-L. Liu, L.-J. Yang, Y. Sun, J.-W. Wang, C.-Q. You and B.-W. Sun, *J. Mater. Chem. C*, 2016, **4**, 8061.
27 K. Kuroiwa, *Inorganics*, 2017, **5**, 45.
28 O. Roubeau, A. Colin, V. Schmitt and R. Clérac, *Angew. Chem., Int. Ed.*, 2004, **43**, 3283.
29 P. Grondin, O. Roubeau, M. Castro, H. Saadaoui, A. Colin and R. Clérac, *Langmuir*, 2010, **26**, 5184.
30 C. Echeverria, M. Rubio, G. R. Mitchell and D. Lopez, *Eur. Polym. J.*, 2014, **54**, 238.
31 T. Fujigaya, D.-L. Jiang and T. Aida, *Chem. – Asian J.*, 2007, **2**, 106.
32 H. Matsukizono, K. Kuroiwa and N. Kimizuka, *J. Am. Chem. Soc.*, 2008, **130**, 5622.
33 I. A. Gural'skiy, C. M. Quintero, G. Molnár, I. O. Fritsky, L. Salmon and A. Bousseksou, *Chem. – Eur. J.*, 2012, **18**, 9946.
34 I. A. Gural'skiy, V. A. Reshetnikov, A. Szebesczyk, E. Gumienna-Kontecka, A. I. Marynin, S. I. Shylin, V. Ksenofontov and I. O. Fristky, *J. Mater. Chem. C*, 2015, **3**, 4737.
35 A. Sanchez-Ferrer, I. Braunlich, J. Ruokolainen, M. Bauer, R. Schepper, P. Smith, W. Caseri and R. Mezzenga, *RSC Adv.*, 2014, **4**, 60842.
36 H. Voisin, C. Aimé, A. Vallée, A. Bleuzen, M. Schmutz, G. Mosser, T. Coradin and C. Roux, *J. Mater. Chem. C*, 2017, **5**, 11542.
37 S. Rat, M. Piedrahita-Bello, L. Salmon, G. Molnár and A. Bousseksou, *Adv. Mater.*, 2018, **8**, 1705275.
38 J. Larionova, L. Salmon, Y. Guari, A. Tokarev, K. Molvinger, G. Molnár and A. Bousseksou, *Angew. Chem., Int. Ed.*, 2008, **47**, 8236.
39 H. Spiering, *Top. Curr. Chem.*, 2004, **235**, 171.
40 Y.-L. Luo, Y. Sun, Q.-L. Liu, L.-J. Yang, G.-J. Wen, M.-X. Wanf and B.-W. Sun, *ChemistrySelect*, 2016, **1**, 3879.
41 M. Rubio, R. Hernández, A. Nogales, A. Roig and D. López, *Eur. Polym. J.*, 2011, **47**, 52.
42 M.-L. Boillot, S. Pillet, A. Tissot, E. Rivière, N. Claiser and C. Lecomte, *Inorg. Chem.*, 2009, **48**, 4729.
43 S.-W. Lee, J.-W. Lee, S.-H. Jeong, I.-W. Park, Y.-M. Kim and J.-I. Jin, *Synth. Met.*, 2004, **142**, 243.
44 I. A. Gural'skiy, C. M. Quintero, J. Sanchez Costa, P. Demont, G. Molnár, L. Salmon, H. J. Shepherd and A. Bousseksou, *J. Mater. Chem. C*, 2014, **2**, 2949.
45 Y.-C. Chen, Y. Meng, Z.-P. Ni and M.-L. Tong, *J. Mater. Chem. C*, 2015, **3**, 945.
46 I. Suleimanov, G. Molnár, L. Salmon and A. Bousseksou, *Eur. J. Inorg. Chem.*, 2017, 3446.
47 Y.-S. Koo and J. R. Galán-Mascarós, *Adv. Mater.*, 2014, **26**, 6785.

48 A. Lapresta-Fernández, M. Pegalajar Cuéllar, J. M. Herrera, A. Salinoas-Castillo, M. del Carmen Pegalajar, S. Titos-Padilla, E. Colacio and L. F. Capitán-Vallvey, *J. Mater. Chem. C*, 2014, **2**, 7292.
49 M. Pegalajar Cuéllar, A. Lapresta-Fernández, J. M. Herrera, A. Salinas-Castillo, M. Del Carmen Pegalajar, S. Titos-Padilla, E. Colacio and L. F. Capitán-Vallvey, *Sens. Actuators, B*, 2015, **208**, 180.
50 A. Tokarev, J. Long, Y. Guari, J. Larionova, F. Quignard, P. Agulhon, M. Robitzer, G. Molnár, L. Salmon and A. Bousseksou, *New J. Chem.*, 2013, **37**, 3420.
51 V. Nagy, I. Suleimanov, G. Molnár, L. Salmon, A. Bousseksou and L. Csóka, *J. Mater. Chem. C*, 2015, **3**, 7897.
52 D. Onggo, I. Mulyani, F. J. Valverde-Munoz, J. A. Real and G. Molnár, *Cellulose*, 2017, **24**, 2205.
53 A. Tsubasa, S. Otsuka, T. Maekawa, R. Takano, S. Sakurai, T. J. Deming and K. Kuroiwa, *Polymer*, 2017, **128**, 347.
54 C. Sanchez, L. Rozes, F. Ribot, C. Laberty-Robert, D. Grosso, C. Sassoye, C. Boissière and L. Nicole, *C. R. Chim.*, 2010, **13**, 3.
55 P. Durand, S. Pillet, E.-E. Bendeif, C. Carteret, M. Bouazaoui, H. El Hamzaoui, B. Capoen, L. Salmon, S. Hebert, J. Ghanbaja, L. Arandah and D. Schaniel, *J. Mater. Chem. C*, 2013, **1**, 1933.
56 C. Faulmann, J. Chahine, I. Malfant, D. de Caro, B. Cormary and L. Valade, *Dalton Trans.*, 2011, **40**, 2480.
57 G. Roy, J. F. Miravet, B. Escuder, C. Sanchez and M. Llusar, *J. Mater. Chem.*, 2006, **16**, 1817.
58 G. Carturan, R. Dal Toso, S. Boninsegna and R. Dal Monte, *J. Mater. Chem.*, 2004, **14**, 2087.